The Role of Stokes drift in Dynamics of Bohai Sea, China under Typhoon Condition

Zengan DENG[1,2,*], Menghan WANG[1] and Yu CAO[1]

[1]School of Marine Science and Technology, Tianjin University, Tianjin 300072, China

[2]Department of Natural Sciences, University of Maryland Eastern Shore, Princess Anne, Maryland 21853, United States

Corresponding author: Zengan DENG (dengzengan@163.com)

Key Points:

- Stokes drift greatly enhances the turbulent mixing at all depths in Bohai Sea under typhoon condition, about 7 times that in normal weather.
- Stokes drift strengthens the sea surface cooling under typhoon condition, the maximum decrease is roughly 7 times that in normal weather.
- The mixed layer depth is increased by ~$O(1)$ during typhoon due to Stokes drift. A hysteretic response presents at the after-typhoon stage.

Abstract

The role of Stokes drift production (SDP), including Coriolis-Stokes forcing, small scale Langmuir circulation and resolved-scale Craik-Leibovich vortex forcing, in ocean dynamics of Bohai Sea (BS), China under typhoon condition is systematically investigated for the first time, utilizing a coupled wave-current modeling system, which is verified to be capable of well simulating the ocean dynamical processes. The effects of SDP on the turbulent mixing and further the dynamics during the entire typhoon period, including the pre-typhoon, during-typhoon, and after-typhoon stages, are comprehensively detected and discussed. Experimental results show that SDP greatly enhances the turbulent mixing at all depths in BS under typhoon condition, the increase can be up to 7 times that of the normal weather. At the same time, SDP generally strengthens the sea surface cooling by more than 0.4℃, with the maximum SST decrease exceeding 2℃ at the during-typhoon stage, about 7 times that in normal weather. SDP-induced current speed decrease can be over 0.2m/s, and change in current direction is generally opposite to the wind direction, suggesting that to a certain extent Stokes drift depresses the impact of high wind speed on current by intensifying the turbulent mixing. MLD is distinctly increased by ~$O(1)$ during typhoon due to SDP, in deep water region the deepening is greater than 5m, and the maxima can be ~7.5m. In addition, the continuous impacts of SDP on SST, current and MLD at the after-typhoon stage present a hysteretic response between SDP and typhoon action.

Keywords: Stokes drift production, Langmuir turbulence, Turbulent mixing, Typhoon, Coupled model

1 Introduction

The surface waves can greatly affect the circulation and thermohaline structures thus modulate the production and dissipation in the upper ocean. Stokes drift production (SDP) and wave breaking have been identified to be two main ways that surface waves affect the upper ocean structures and dynamics. Previous studies (Noh et al., 2004; Kantha & Clayson, 2004; Li et al., 2013) have proved that the wave breaking effect is limited within several meters immediately below the ocean surface. It's widely confirmed that Stokes drift plays a key role in upper ocean dynamic and thermal mechanism. SDP affects the turbulent mixing of upper ocean principally via large scale Coriolis-Stokes forcing (CSF), small scale Langmuir circulation (LC) and resolved-scale Craik-Leibovich vortex forcing (CLVF). Due to SDP (refers to CSF, LC and CLVF thereafter), the instability of the vertical shear of the upper ocean tends to be increased and the momentum and heat will penetrate into the deeper depths, making the mixed layer thicker.

By introducing the Stokes drift, many modifications have been put forward based on the Mellor-Yamada closure scheme (M-Y2.5), a typical second-moment turbulent closure model, to improve the parameterization of turbulent mixing. Kantha and Clayson (2004, KC04) added the kinetic energy induced by LC into the M-Y2.5 parameterization, and solved the issue that the simulated mixing layer is too thin. Harcourt (2015, H15) adopted inhomogeneous pressure-strain rate as well as pressure-scalar gradient closures and modified the stability function in the second-moment model to match CLVF term. Based on above improved parameterizations, the mechanisms between wave processes and upper ocean thermal structures under normal weather were discussed (Li et al., 1993; Sun et al., 2003; Polton et al., 2007; Zhang et al., 2012; McWilliams et al, 2012; LI et al., 2013; Pearson et al, 2015), suggesting that LC can enhance the upper ocean mixing notably.

Typhoon, as an extreme weather event, drastically exerts on the ocean surface, induces intense waves with wave height up to 15m and drives strong currents with speed as large as >1m/s (Ginis et al., 2002). As a consequence, thermohaline structures can be greatly changed. As the direct contributor to the typhoon energy budget, sea-air flux remarkably dictates the typhoon intensity (Emanuel et al., 1999). Both SSTs and currents are used to calculate sea-air heat and momentum fluxes in the typhoon prediction models. The responses of SST and current to typhoon are significantly determined by the upper-ocean turbulent mixing. Thus, it's necessary to accurately estimate the turbulent mixing, in particular the wave-induced part, under the extreme weather condition of typhoon. The effects of wave-induce mixing on thermal response to typhoon in the Yellow and East China Seas, South China Sea and east of the Luzon Strait had been discussed previously (Zhang et al., 2017; Li et al., 2014; Zhang et al., 2012). However, the combination impacts of SDP (CSF, LC, CLVF) on turbulent mixing and ocean dynamics under typhoon conditions have never been comprehensively studied in BS. The main reason for this could be that the tropical storms can not easily reach BS region.

BS with shallow depth but complex topography locates on the west coast of the Pacific Ocean, composed of the Liaodong Bay, the Bohai Bay, the Laizhou Bay and the Central Sea Area (Fig. 1(a)). Extra-tropical storm and coldwaves often pass through and influence this region, and typhoon can hit infrequently. BS has some important ports including Tianjin Port and Dalian Port, and it's close to megacities, such as Beijing and Tianjin. Once typhoon/storm surge occurs, coastal cities may suffer from serious economic loss, which inspires us to investigate the role of SDP in dynamic processes in BS under typhoon condition, based on which more accurately prediction model for disaster mitigation could be further developed.

In this study we simulate the influences of SDP on turbulent mixing under typhoon condition, and further detect the responses of ocean dynamics to the actions of typhoon in the presence of SDP effects. In our parameterization, Langmuir turbulence

(via LC) is included in the turbulence model and both CSF and resolves-scale CLVF are added into the momentum equations of the ocean model. Case study of supertyphoon Matsa (2005) is then presented and discussed.

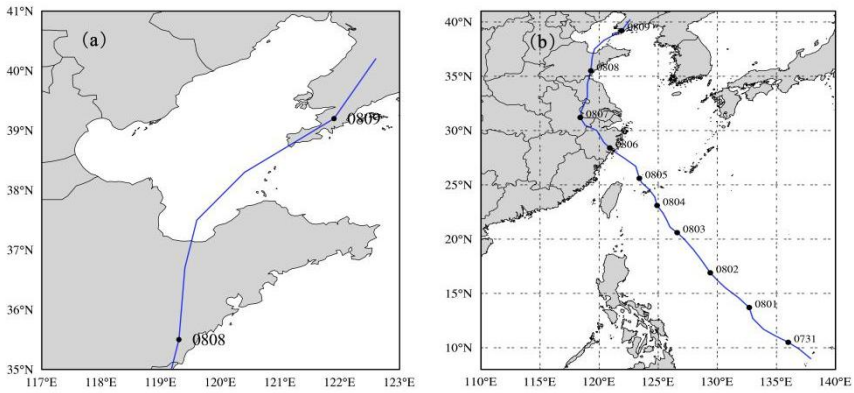

Figure 1. (**a**) The geographic location of BS; (**b**) The path (blue line) of supertyphoon Matsa in August 2005.

2 Methods

An one-way coupled wave-current modeling system (Fig. 2) is constructed by combination of the Princeton Ocean Model with the generalized coordinate system (POMgcs, Ezer & Mellor 2004) and the Simulating Waves Nearshore model (SWAN, Booij et al., 1999). The Stokes drift is calculated by wave variables output from SWAN and then introduced to POMgcs to represent SDP. The specific scheme is given in following sub-sections.

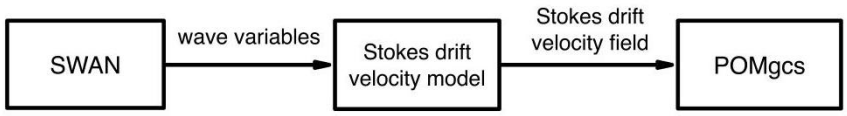

Figure 2. A brief diagram of the wave-current modeling system, illustrating the inputs and outputs among different modules.

112 2.1 Ocean current model

113 POMgcs, developed based on the Princeton Ocean Model (POM; Blumberg &
114 Mellor, 1987), is a 3-D, primitive-equation, free-surface, coastal circulation model, in
115 which the Mellor-Yamada 2.5 turbulence closure scheme is included. It has been widely
116 used to simulate the ocean current/circulation.

117 When CSF and the resolved-scale CLVF are considered, the horizontal
118 momentum equations in POMgcs can be modified as follows (McWilliams & Restrepo,
119 1999; Reichl et al., 2016; Cao & Deng, 2019):

120 $$\frac{\partial Us_k}{\partial t}+\frac{\partial U^2 s_k}{\partial x}+\frac{\partial UVs_k}{\partial y}+\frac{\partial U\omega}{\partial k}-fVs_k+gs_k\frac{\partial \eta}{\partial x}+g\frac{s_k}{\rho_0}\int_k^0[s_k\frac{\partial \rho'}{\partial x}-(s_x+\eta_x)\frac{\partial \rho'}{\partial k'}]\,dk'$$

121 $$=\frac{\partial}{\partial k}[\frac{K_M}{s_k}\frac{\partial U}{\partial k}]+F_x+CSFX+CLVFX$$

122 (1)

123 $$\frac{\partial Vs_k}{\partial t}+\frac{\partial V^2 s_k}{\partial y}+\frac{\partial UVs_k}{\partial x}+\frac{\partial V\omega}{\partial k}+fUs_k+gs_k\frac{\partial \eta}{\partial y}+g\frac{s_k}{\rho_0}\int_k^0[s_k\frac{\partial \rho'}{\partial y}-(s_y+\eta_y)\frac{\partial \rho'}{\partial k'}]\,dk'$$

124 $$=\frac{\partial}{\partial k}[\frac{K_M}{s_k}\frac{\partial V}{\partial k}]+F_y+CSFY+CLVFY$$

125 (2)

126 with

127 $$s_x=\frac{\partial s}{\partial x},\ s_y=\frac{\partial s}{\partial y},\ \eta_x=\frac{\partial \eta}{\partial x},\ \eta_y=\frac{\partial \eta}{\partial y},\ s=z-\eta \quad (3)$$

128 $$CSFX=fV_s s_k \quad (4)$$

129 $$CSFY=-fU_s s_k \quad (5)$$

130 $$CLVFX=Vs[s_k(\frac{\partial V}{\partial x}-\frac{\partial U}{\partial y})-(s_x+\eta_x)\frac{\partial V}{\partial k}+(s_y+\eta_y)\frac{\partial U}{\partial k}] \quad (6)$$

131 $$CLVFY=-Us[s_k(\frac{\partial V}{\partial x}-\frac{\partial U}{\partial y})-(s_x+\eta_x)\frac{\partial V}{\partial k}+(s_y+\eta_y)\frac{\partial U}{\partial k}] \quad (7)$$

132 where x, y are the horizontal coordinates, k is the vertical coordinate, s_k is the kth

level thickness, ω is the vertical velocity, (U, V) are the horizontal components of the Eulerian mean current with (Us, Vs) the horizontal components of Stokes drift, f is the Coriolis parameter, ρ_o is the reference water density and ρ' is the density deviation, K_m is the vertical mixing coefficient, F_x is the horizontal viscosity term and F_y is the horizontal diffusion term. ($CSFX$, $CSFY$) are the horizontal components of CSF, respectively. ($CLVFX$, $CLVFY$) are the horizontal components of CLVF, respectively.

The parameterization H15, which is based on M-Y2.5, is introduced to represent LC. By considering the LC, the turbulent kinetic energy (TKE) and turbulent length scale equations are modified to as follows:

$$\frac{\partial q^2 s_k}{\partial t} + \frac{\partial U q^2 s_k}{\partial x} + \frac{\partial V q^2 s_k}{\partial y} + \frac{\partial \omega q^2}{\partial k} - \frac{\partial}{\partial k}\left[\frac{K_q}{s_k}\frac{\partial q^2}{\partial k}\right]$$

$$= -\frac{2}{s_k}\overline{u\omega}\left(\frac{\partial U}{\partial k} + \frac{\partial U_s}{\partial k}\right) - \frac{2}{s_k}\overline{v\omega}\left(\frac{\partial V}{\partial k} + \frac{\partial V_s}{\partial k}\right) + \frac{2g}{\rho_0}K_H\frac{\partial \tilde{\rho}}{\partial k} - 2\frac{s_k q^3}{B_1 l} + F_q \quad (8)$$

$$\frac{\partial q^2 l s_k}{\partial t} + \frac{\partial U q^2 l s_k}{\partial x} + \frac{\partial V q^2 l s_k}{\partial y} + \frac{\partial \omega q^2 l}{\partial k} - \frac{\partial}{\partial k}\left[\frac{K_q}{s_k}\frac{\partial q^2 l}{\partial k}\right]$$

$$= \frac{E_1 l}{s_k}\left(-\overline{u\omega}\frac{\partial U}{\partial k} - \overline{v\omega}\frac{\partial V}{\partial k}\right) + \frac{E_6 l}{s_k}\left(-\overline{u\omega}\frac{\partial U_s}{\partial k} - \overline{v\omega}\frac{\partial V_s}{\partial k}\right) + E_1 E_3 l\frac{g}{\rho_0}K_H\frac{\partial \tilde{\rho}}{\partial k} - \frac{s_k q^3}{B_1}\tilde{W} + F_l \quad (9)$$

with

$$\overline{u\omega} = -\left(K_M\frac{\partial U}{\partial k} + K_{MS}\frac{\partial U_s}{\partial k}\right) \quad (10)$$

$$\overline{v\omega} = \left(K_M\frac{\partial V}{\partial k} + K_{MS}\frac{\partial V_s}{\partial k}\right) \quad (11)$$

$$K_{MS} = qlS_{MS} \quad (12)$$

where q is TKE, l is turbulence length scale, K_H and K_q are the vertical diffusion coefficients for temperature and turbulence kinetic energy, $\tilde{\rho}$ is the corrected density, $\tilde{W}$ is the wall proximity function, F_q is the horizontal diffusion terms for TKE and F_l is for turbulence length scale. Model constants E_1=E_3=1.8, B_1=16.6, following Mellor and

Yamada (1982). E_6 is a new parameter related LT and its value equal to $4E_1$ following KC04. $\overline{u\omega}$ and $\overline{v\omega}$ are vertical turbulent flux term. K_{MS} is a new vertical kinematic viscosity coefficient derived from the new stability function S_{MS} in H15.

The modeling domain covers the whole BS region ranging from (37.083°N, 117.52°E) to (41.033°N, 122.47°E). The horizontal resolution is 1/20°×1/20°, which is thought to be fine enough for resolving the associated processes in this study. The water depth of the modeling region is represented by ETOPO2 topography dataset derived from National Oceanic and Atmospheric Administration (NOAA). 6 terrain-following coordinates are specified in the vertical, and all of the model outputs are interpolated to 6 standard z-levels, i.e. 0m, 5m, 15m, 25m, 35m, and 65m. The internal-mode time step of the current model is 200s, and external-mode time step is 3.33s.

The model initialization fields consist of temperature, salinity and current velocity, obtained from the China Ocean Reanalysis (CORA). The integration time of diagnostic experiments is spanning from 7 August to 10 August 2005, covering the entire duration that supertyphoon Matsa passed BS. A stable current field is achieved by spun up the current model for half a year. The simulation is forced by both heat fluxes and winds, derived from the European Centre for Medium-Range Weather Forecasts (ECMWF) and the National Centers for Environmental Prediction (NCEP), respectively. In addition, the tidal elevation forcing at the open lateral boundaries includes four main tidal components of M_2, S_2, K_1 and O_1, derived from a 3-D tidal model (Han et al., 2006).

2.2 Ocean wave model

SWAN is a third-generation wave model based on spectral action balance equation, adopting the linear random gravity waves theory. It was widely used to simulate the regional sea surface waves. The modeling domain, topography, wind

forcing, horizontal resolution and time step (200s) for wave simulations are all consistent with those used in current model. The output time interval of wave variables is 1h.

2.3 Typhoon winds and Stokes drift

Super-typhoon Matsa is selected as the representative study case, provided that there were not many strong typhoons can visit BS, and Matsa was one of the biggest. The wind field of Matsa is from the ECMWF dataset. Fig. 1(b) shows the Matsa's traveling path. Matsa was generated in the east of Philippines on 31 July 2005, developed to a strong typhoon on 4 August and made landfall in Zhejiang Province, China on 6 August. It entered BS on 8 August and weakened to an extra-tropical cyclone the day after. The influence time interval of Matsa in BS was mainly from 8 ~9 August 2005, when the maximum wind speed exceeded 20m/s. We are focusing on the period from 7~10 August 2005, covering the time frame from pre-typhoon stage to after-typhoon stage. Four plots in Fig. 3 respectively display the horizontal distribution of the 10-m winds at 0000 UTC from 7~10 August 2005.

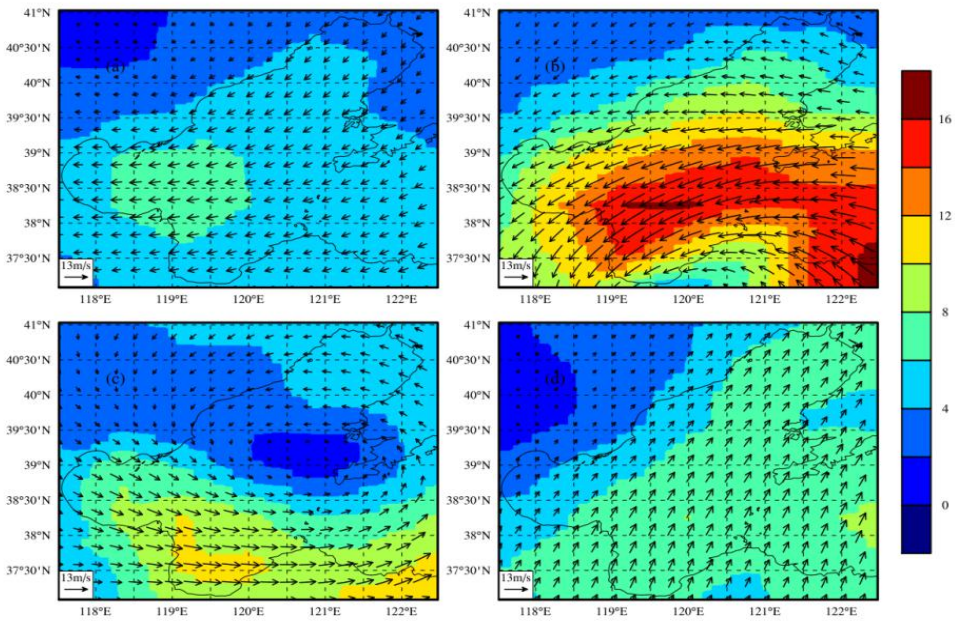

Figure 3. Horizontal distribution of 10-m wind direction and speed at 0000 UTC on (**a**)7th, (**b**)8th, (**c**)9th and (**d**)10th August 2005

196 The Stokes drift is calculated from the wave spectrum (Webb & Fox-Kemper,
197 2011) through the following equation:

198 $$U_s(z) = \frac{16\pi^3}{g}\int_0^{\infty}\int_{-\pi}^{\pi}(\cos\theta, \sin\theta, 0) f^3 S_{f\theta}(f,\theta) e^{\frac{8\pi^2 f^2}{g}} \mathrm{d}\theta \mathrm{d}f \quad (13)$$

199 where $S_{f\theta}$ is the wave frequency-direction spectrum with θ the wave direction and
200 f the wave frequency. The calculated Stokes drift from simulated wave variables is given
201 in Fig. 4, showing that the direction of Stokes drift basically agrees with wind direction
202 and the Stokes drift speed is positively correlated to wind speed, except when a complete
203 typhoon cyclone has formed in BS on 9 August.

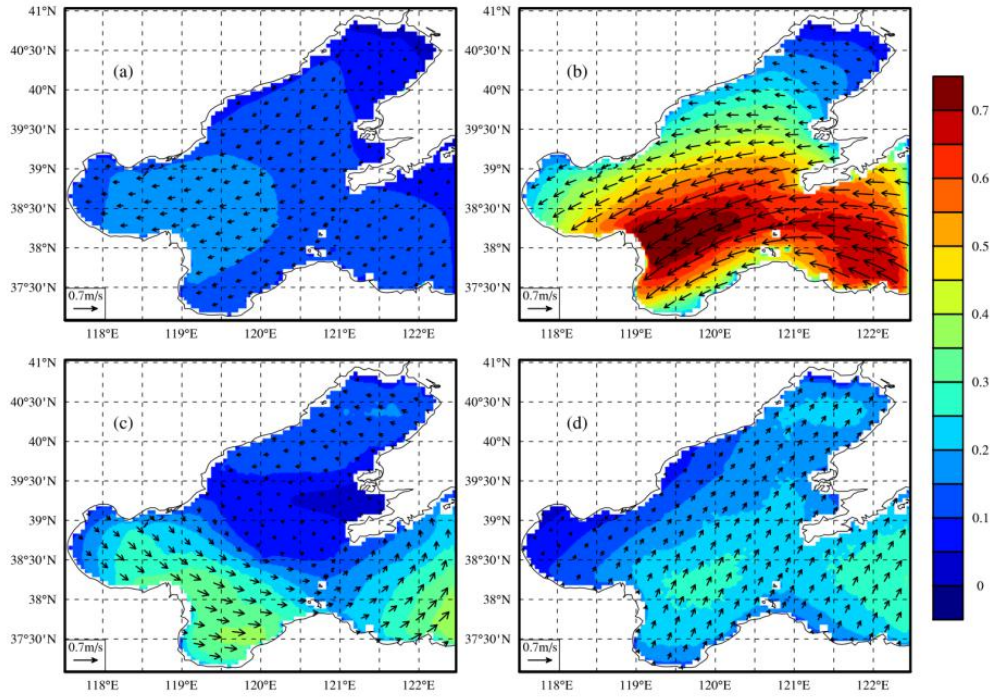

204

205 **Figure 4**. Horizontal distribution of Stokes drift direction and speed at 0000 UTC on (**a**)
206 7th , (**b**)8th , (**c**)9th and (**d**)10th August 2005

207

208

209 **3 Model verification**

210 Our simulations is validated via the comparison of tidal constants. The tidal
211 constants from observations at 8 tidal stations (Table 1) in BS are compared to the tidal
212 constants analyzed from the simulations performed by our modeling. Fig. 5 gives the
213 fitted results of observed and simulated tidal amplitude for M_2 and K_1, showing a
214 favorably good agreement. The corresponding tidal phase-lag also agrees well, denoting
215 that there are no noticeable systematic errors exist in the simulations. These analyses
216 demonstrate that the modeling is basically reliable.

217

218 **Table1**. Locations of eight tidal stations in BS

Number	Station	latitude/°N	longitude/°E
1	Xiaoqinghekou	37.33	119.06
2	Yantai	37.55	121.38
3	Longkou	37.65	120.32
4	North Huangchengdao	38.40	120.92
5	Lalian	38.87	121.68
6	Tanggu	38.98	117.78
7	Changxingdao	39.65	121.47
8	Tuanshanjiao	40.23	120.47

219

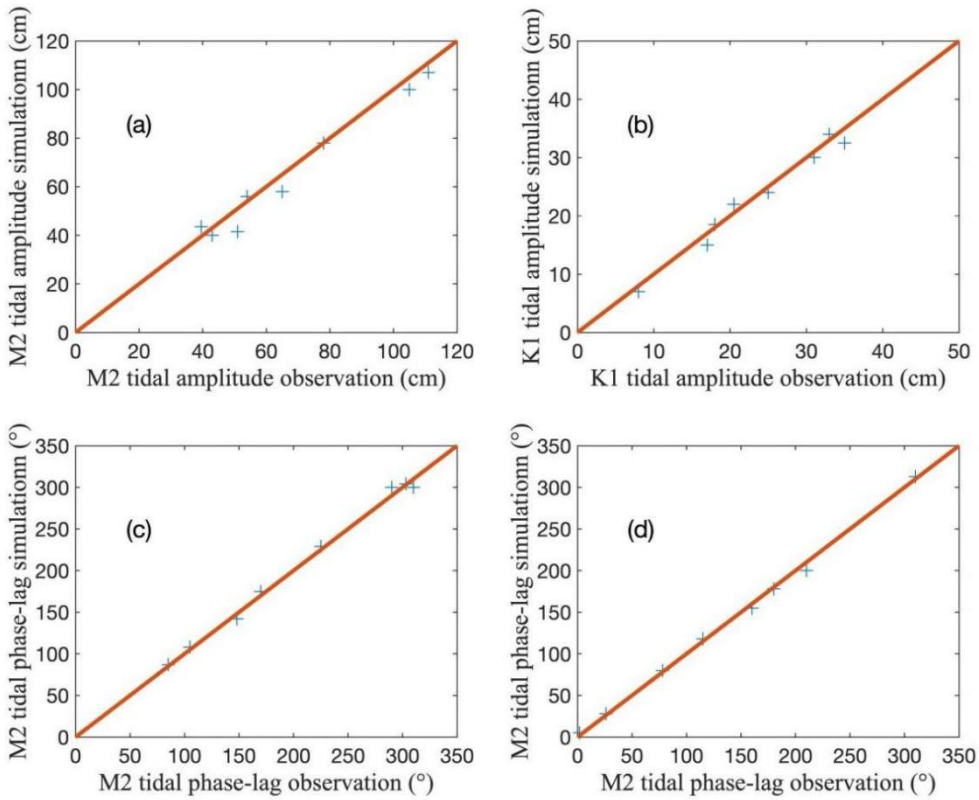

Figure 5. Fitted plots of observed amplitude and simulated amplitude of (**a**) M_2, (**b**) K_1 and observed phase-lag and simulated phase-lag of (**c**) M_2, (**d**) K_1.

4 Results

In our previous study (Cao & Deng, 2019), the specific effects of each SDP term (LC, CSF and CLVF) on ocean dynamics in normal weather have been comprehensively investigated and compared to each other, therefore we are not repeat this work again in typhoon condition given the limit of paper length. Two sets of diagnostic experiments are designed and conducted: WAVE-ALL, including all SDP terms; and WAVE-NON, without SDP. The WAVE-NON acts as coordinate/reference experiment, and the responses of ocean processes to typhoon as well as the impacts of SDP on turbulent mixing and ocean dynamics are detected by comparing the simulations of WAVE-NON with that of WAVE-ALL. We present and discuss our results in detail at 3 stages, i.e. pre-typhoon, during-typhoon and after-typhoon.

Before investigating the influences of SDP on SST, current and MLD, it's essential to figure out its effects on vertical turbulent mixing under typhoon condition. K_M is the vertical kinetic viscosity coefficient from WAVE-NON, and K_{MS} is that from WAVE-ALL. Fig. 6(a) shows the monthly-mean vertical kinetic viscosity coefficient under normal weather (June 2005), adopted from our previous study (Cao & Deng, 2019). The mixing coefficient at the pre-typhoon stage on 7 August (Fig. 6(b)) is generally consistent to that of the normal weather (Fig. 6(a)), the difference between them is generally less than $0.0012m^2/s$. The slightly differences at 5m and 15m levels between Fig. 6(a) and Fig. 6(b) may be resulted from the more stably vertical stratification in August 2005. The impacts of Stokes drift on upper ocean mixing tend to be strengthened as the increase of depth, indicating that the waves can generally penetrate into the whole depth in BS. At the during-typhoon stage (8 August), the mixing coefficients (both K_M and K_{MS}) are greatly improved by about 1 order of magnitude, demonstrating that strong winds enable a large amount of TKE inject down to the deep, as a consequence of turbulent mixing enhance (Fig. 6(c)). Adding the SDP, the vertical kinetic viscosity coefficient is further increased. The difference between K_M and K_{MS} exceeds $0.008m^2/s$, about 7 times that of the normal weather, denoting the very important role of Stokes drift in turbulent mixing under typhoon condition. The Stokes drift influences on mixing at during-typhoon stage are relatively strong in the upper 30m (Fig. 6(c)), whereas the effects are stronger within 30~50m at the pre-typhoon stage (Fig. 6(b)). At the after-typhoon stage (10 August), TKE injection is markedly decreased. As a result, K_M and K_{MS} generally decrease to the magnitude at pre-typhoon stage, however the values (Fig. 6(d)) are still larger than that in normal weather (Fig. 6(a) and 6(b)), suggesting that K_M and K_{MS} are gradually recovering to the level before typhoon. The deviation between K_M and K_{MS} on 10 August is similar to that at the pre-typhoon stage, with the maximum of $\sim 0.001m^2/s$ appearing at 15m-layer, shallower than that at the pre-typhoon stage. The depth with maximum Stokes influence may transmit from the

15m-layer to deeper layers in few days and the impacts of Stokes drift will gradually recover to the level before typhoon.

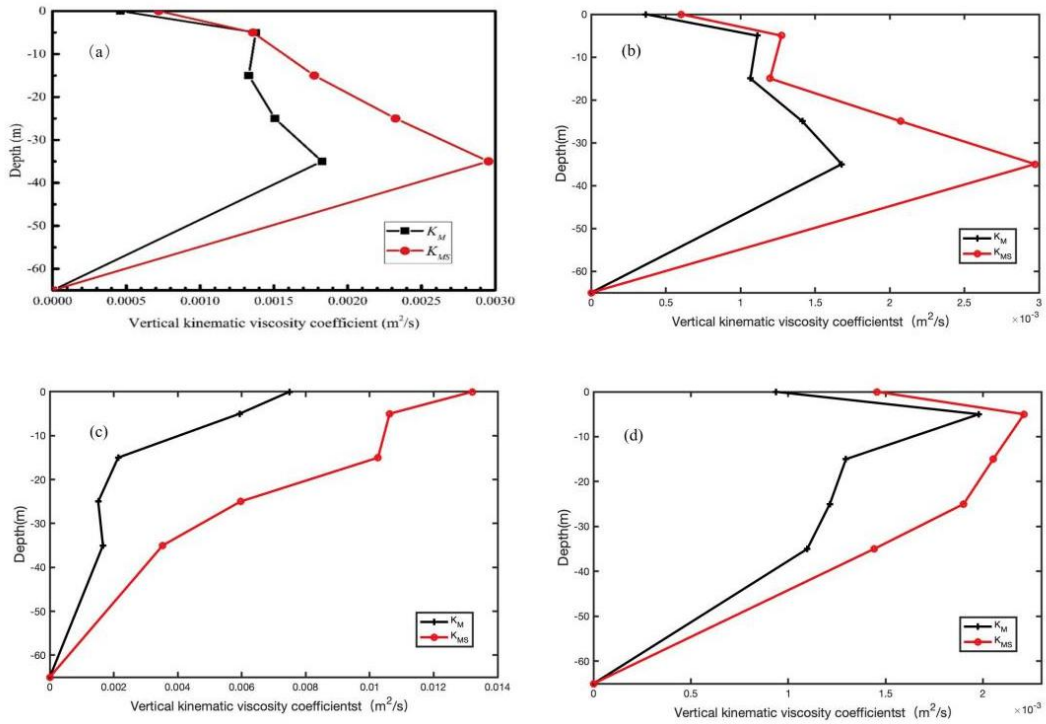

Figure 6. Vertical kinetic viscosity coefficient (**a**) in normal weather (adopted from Cao and Deng, 2019); Vertical kinetic viscosity coefficient simulated at 0000UTC on (**b**) 7th, (**c**)8th and (**d**)10th August 2005 in this study. (K_M is the kinetic viscosity coefficient from WAVE-NON, and K_{MS} is that from WAVE-ALL)

4.1 Pre-typhoon stage

This stage was before 8 August 2005, when Masta was close to but hadn't entered into BS. The horizontal distributions of SST simulated by WAVE-NON and WAVE-ALL on 7 August are shown in Fig. 7(a) and Fig. 7(b), respectively. Fig. 7(c) gives the difference of SST between the two simulations. SST from WAVE-ALL is lower than that from WAVE-NON in most of the region, indicating that SDP generally decreases the SST. Especially in the southern part of Liaodong Bay, the eastern part of the Bohai Bay, and Miaodao Islands, the SST reduction reaches ~0.3°C. This is similar to the summer case in normal weather previously discussed by Cao & Deng (2019). The

277 difference in percentage (Fig. 7(d)) shows that larger changes appear near the Laizhou
278 Bay and the Bohai Bay, and the maxima can be ~1.8%. In most of BS area, the effect of
279 Stokes drift on SST is less than 0.4%, suggesting that the impact is relatively slight at the
280 pre-typhoon stage, like that in the normal weather.

281 MLD is defined as the depth of the water layer at a temperature difference of
282 0.5°C from the sea surface following Yablonsky and Ginis (2008). The profile along
283 38.33°N, as the widest section crossing BS, is plotted to demonstrate the spatial
284 variability of MLD. Fig. 8(a) shows that in most of the coastal water the mixed layer
285 penetrates deep down to sea floor, indicating that water is well mixed. When longitude
286 exceeds 119°E, MLD decreases rapidly and remains stably at ~1m. It is due to the
287 obviously vertical stratification of temperature in summer and the marked temperature
288 difference between surface and subsurface. In WAVE-ALL, the mixed layer is deepened
289 slightly. However, this amount of change is negligible comparing to the entire water
290 depth, denoting that the impact of Stokes drift is relatively weak under low-wind
291 conditions.

292 Currents on 7 August mainly flow from Liaodong Bay, the Bohai Bay and the
293 Bohai Strait towards the Central Area and the Laizhou Bay (bottom four panels in Fig. 7).
294 The direction of current is largely controlled by winds and tides. As shown in Fig. 7(g),
295 SDP slightly influences the surface current speed, with the maximum alternation being
296 less than ±0.02m/s. Change of ~10% (Fig. 7(h)) occurs in the Central Area, due to the
297 very small local current speeds. The most region of BS is changed by ~±5%. The vertical
298 current speed profile along the 38.333°N section (Fig. 9(a) and 9(b)) also reveals that
299 speeds are slightly reduced at almost all depths, to a certain extent rendering the currents
300 more evenly distributed in the vertical.

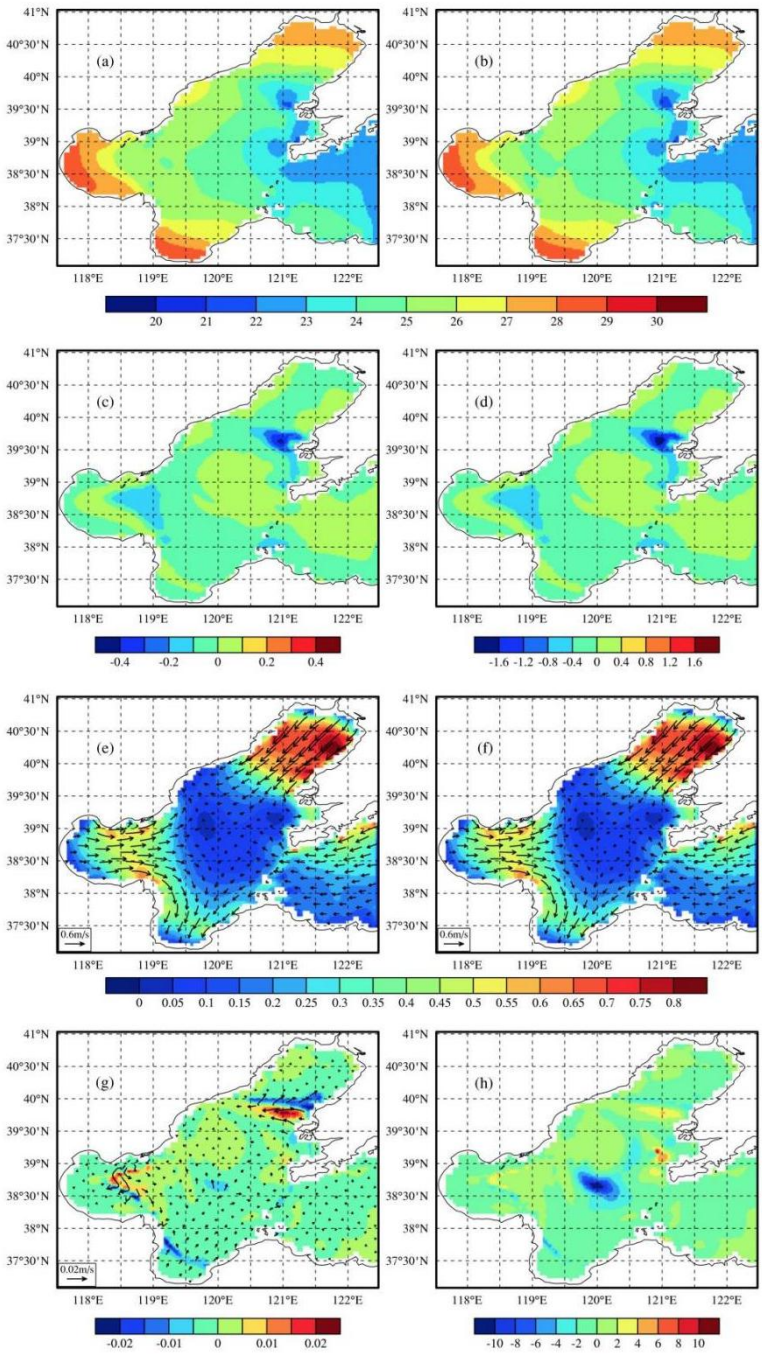

Figure 7. Horizontal distribution of (**a**) SST from WAVE-NON, (**b**) SST from WAVE-ALL, (**c**) SST difference between WAVE-NON and WAVE-ALL, (**d**) SST difference in percentage (%) between WAVE-NON and WAVE-ALL, (**e**) current from WAVE-NON, (**f**) current from WAVE-ALL, (**g**) current difference between WAVE-NON and WAVE-ALL, (**h**) current difference in percentage (%) between WAVE-NON and WAVE-ALL at 0000UTC on 7 August 2005. (Contours depict the current speed, while arrows represent the direction of current.)

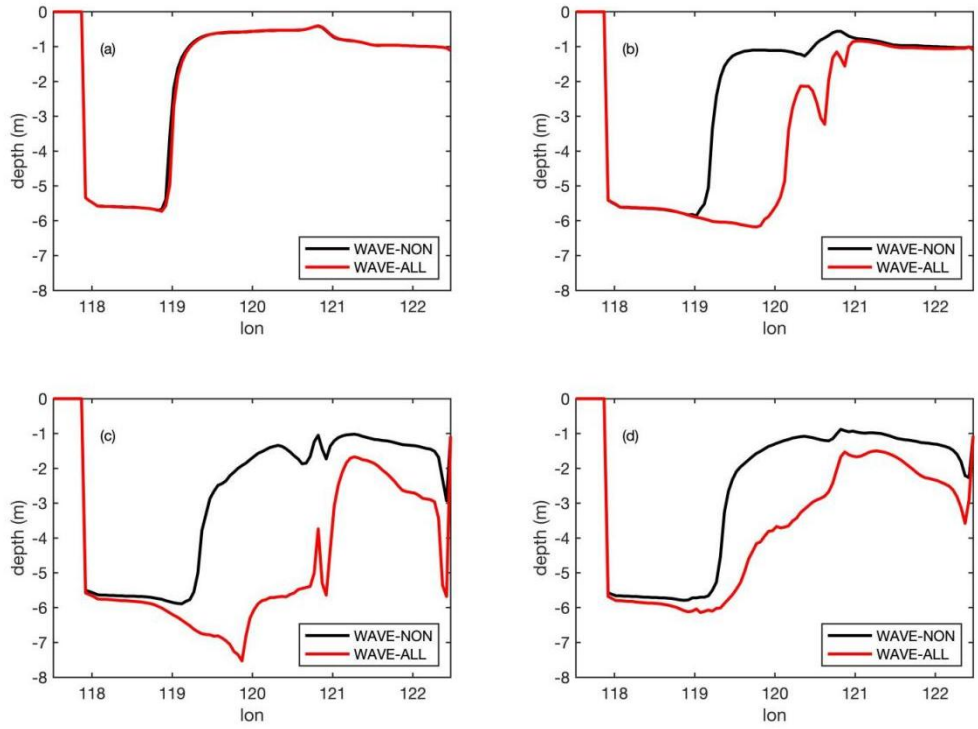

309

310 **Figure 8**. MLD from WAVE-NON and WAVE-ALL along the 38.333°N section at
311 0000UTC on (**a**) 7th , (**b**) 8th , (**c**) 9th , (**d**)10th August 2005

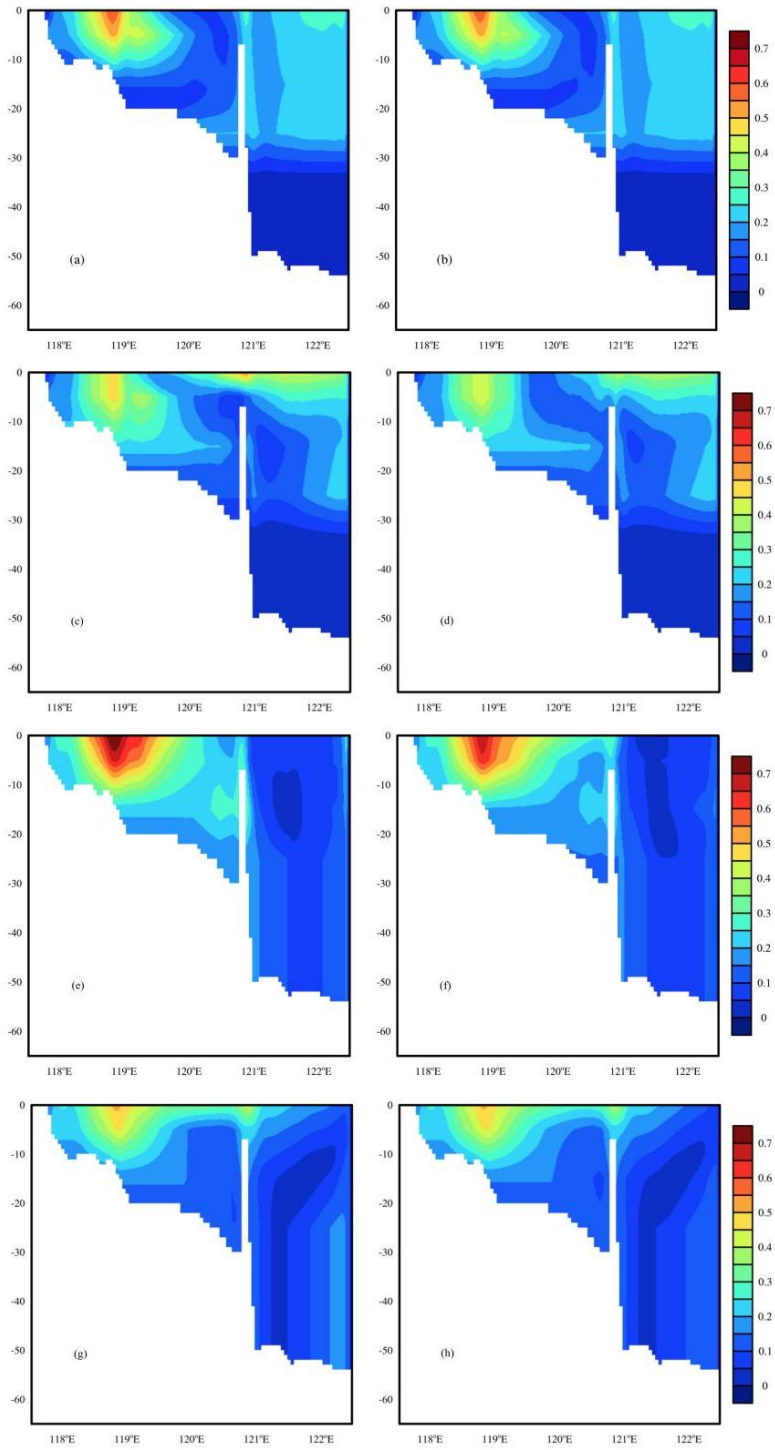

312

313 **Figure 9**. Vertical current speed profile along the 38.333°N from WAVE-NON (left) and
314 WAVE-ALL (right) at 0000UTC on 7th (**a**, **b**), 8th (**c**, **d**), 9th (**e**, **f**), 10th (**g**, **h**) August 2005

315

316 4.2 During-typhoon stage

317 When Matsa entered BS on 8 August, the typhoon-induced cooling is great along
318 the typhoon traveling path. The SST is rapidly decreased for more than 2℃ (Fig. 10(a))
319 compared to that on 7 August (Fig. 7(a)). The difference of SST between WAVE-NON
320 and WAVE-ALL reaches a maximum of ~1.4℃ (Fig. 10(c)), the change is much larger
321 than that at the pre-typhoon stage (Fig. 7(c)). The rate of SST change reaches ~6%, about
322 $O(1)$ larger than that at the pre-typhoon stage. Reichl et al. (2016) have demonstrated
323 that the total air-sea heat flux can be reduced by at least 10% with the decrease of 0.5°C
324 in SST. Fig. 10(c) shows that SDP promotes the lifting of deeper cold water, resulting in
325 an additional cooling at the surface, and Matsa largely strengthens the effect of SDP on
326 ocean thermal processes, leading to obviously SST reduction and noticeably enlarged
327 cooling range.

328 One day after Matsa entered BS (9 August), a greater range and intensity of
329 cooling is further caused (Fig. 10(e)). SST is generally reduced by the action of SDP (Fig.
330 10(f)). The temperature changes in the Central Area and the Bohai Strait are noticeable,
331 with the maxima of more than 2°C and the alternation in percentage exceeding 10% (Fig.
332 10(g) and 10(h)), because the relatively large water depth in this region facilitates the
333 pulling of deeper cold water up to the surface by SDP effects. Although the intensity of
334 winds on 9 August is significantly weakened compared to 8 August, the subsequent
335 change of heat flux in the vertical caused by SDP is still existing, leading to a hysteretic
336 change in SST.

337 MLD in the deep water region (approximately from 119°E to 121°E) is distinctly
338 increased by ~5m on 8 August (Fig. 8(b)) due to SDP. The increase of MLD in the
339 region from 121°E to 122.5°E is small, as the small SST difference in this area (Fig.
340 7(c)). Because of the continuously forcing of typhoon winds, the mixed layer is further
341 deepened, with MLD in deep water region being greater than 3m, and the largest one
342 reaching ~7.5m (Fig. 8(c)). However, on the contrary, MLD is rapidly decreased in the

343 vicinity of the typhoon center, which is consistent with the result given by Reichl et al.
344 (2016). Taking consideration of Stokes drift, MLD is generally deepened by ~$O(1)$.

345 The surface current is strengthened, especially in the Bohai Strait and the Central
346 Area where the wind speed of typhoon is relatively high (top four panels in Fig. 11). The
347 current velocity in the Liaodong Bay, where was not affected by typhoon, basically
348 equals to that on 7 August (Fig. 11(a)). The maximum of Stokes drift-induced surface
349 current speed decrease exceeds 0.2m/s, a huge impact evidenced in Fig. 11(d). The area
350 with largest current speed change (Fig. 11(c)) coincides to the region with the most
351 significant SST alternation (Fig. 10(c)), demonstrating that in this area SDP plays a
352 greater role in vertical turbulent mixing and TKE.

353 Comparing to the vertical current profile on 7 August (Fig. 9(a)), Matsa forces
354 the currents more evenly distributed within the entire shallow depth (Fig. 9(c)) on 8
355 August. The including of SDP further reduces the current speed at the whole depth in BS
356 (Fig. 9(d)). However, owing to the short duration of typhoon action, the TKE transmitted
357 from the atmosphere to the ocean is mainly limited to a depth of a few meters right
358 below the sea surface. Therefore, the vertical current is stratified in the Central Area and
359 the Bohai Strait, with large velocity difference between surface and deep waters.

360 On 9 August, one day after Masta intruded BS, the surface current speed is
361 prominently decreased by about 0.3m/s in the region with high wind speed (Fig. 11(e)).
362 Current is wholly directed to Laizhou Bay before typhoon, and flows basically along
363 wind direction at the during-typhoon stage, illustrating that under typhoon condition
364 wind is the dominant factor in controlling the ocean dynamics, even more important than
365 tidal current. The influence of SDP on the current is further enhanced, and the current is
366 generally weakened, particularly in northern Laizhou Bay. The maximum alternation in
367 percentage (Fig. 11(h)) exceeds 100%, owing to the small current speed in the Central
368 Area. The Stokes-induced differences in current direction between 8 and 9 August
369 (shown in Fig. 11(c) and 11(g)) are both generally opposite to the wind direction,

370 suggesting that at a certain degree the Stokes drift depresses the effect of strong winds on
371 currents by strengthening the vertical turbulent mixing.

372 The current speed in the upper and lower layers is similar and the energy
373 transported from the atmosphere to the ocean can fully inject into the whole depth (Fig.
374 9(e)). As a result of typhoon wind, currents generally flow along the same direction, and
375 the current speed is increased obviously in the Bohai Bay and the Central Area (Fig. 9(c)
376 and 9(e)). In contrast, the current speed is small in the Bohai Strait owing to it's close to
377 the typhoon center and the opposite direction between wind and circulation. Adding the
378 SDP, the vertical distribution of current speed (Fig. 9(e) and 9(f)) is noticeably changed,
379 its magnitude is generally decreased.

380

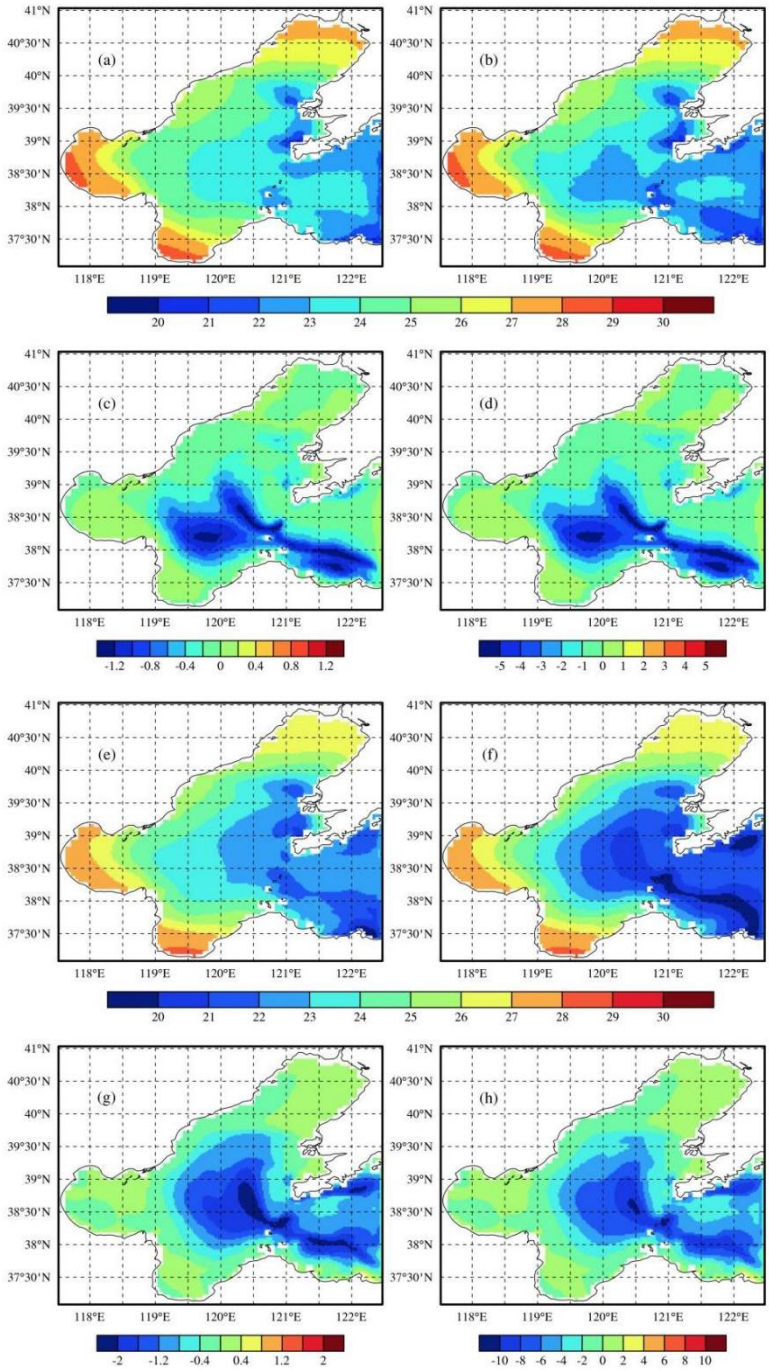

Figure 10. Horizontal distribution of (**a**) SST from WAVE-NON, (**b**) SST from WAVE-ALL, (**c**) SST difference between WAVE-NON and WAVE-ALL, (**d**) SST difference in percentage (%) between WAVE-NON and WAVE-ALL at 0000UTC on 8 August 2005 and (**e**) SST from WAVE-NON, (**f**) SST from WAVE-ALL, (**g**) SST difference between WAVE-NON and WAVE-ALL, (**h**) SST difference in percentage (%) between WAVE-NON and WAVE-ALL at 0000UTC on 9 August 2005.

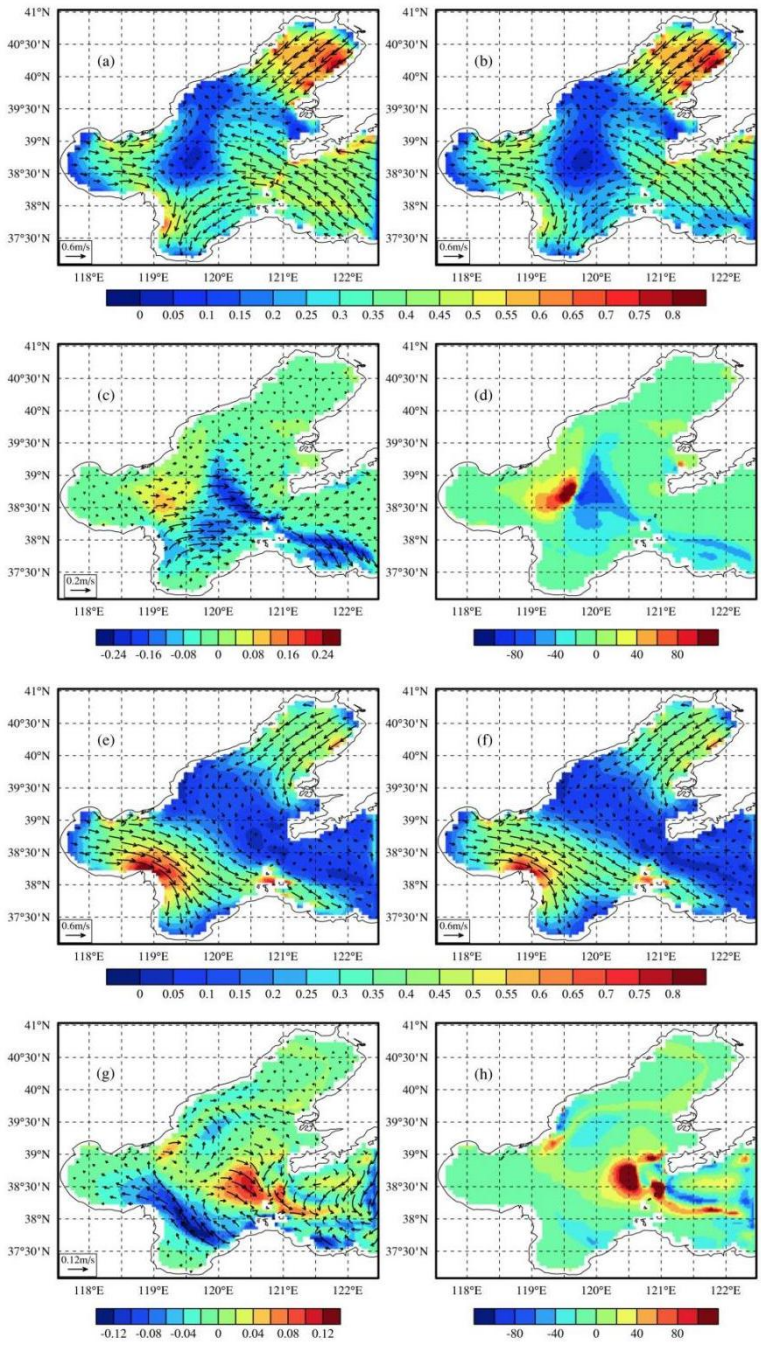

Figure 11. Horizontal distribution of (**a**) current from WAVE-NON, (**b**) current from WAVE-ALL, (**c**) current difference between WAVE-NON and WAVE-ALL, (**d**) current difference in percentage (%) between WAVE-NON and WAVE-ALL at 0000UTC on 8 August 2005 and (**e**) current from WAVE-NON, (**f**) current from WAVE-ALL, (**g**) current difference between WAVE-NON and WAVE-ALL, (**h**) current difference in percentage (%) between WAVE-NON and WAVE-ALL at 0000UTC on 9 August 2005.

395 4.3 After-typhoon stage

396 Matsa was weakened to an extra-tropical cyclone after 9 August. At this stage,
397 SST rises gradually from 10 August (Fig. 12(a)) and later on. However, compared to the
398 results on 7 August (Fig. 7(a)), SST is not fully recovered to the level before typhoon.
399 SDP mainly reduces SST in the Bohai Strait and the Central Area, and the extent and
400 range of the decreases (Fig. 12(c) and 12(d)) are similar to that on 9 August (Fig. 10(g)
401 and 10(h)). The additional cooling at the after-typhoon stage indicates that SDP can not
402 only affect SST at synoptic time scale, but also could impact the total heat budget at
403 longer time interval. Without strong typhoon winds, MLD is decreased from 10 August.
404 MLD simulated from WAVE-All is deeper than that from WAVE-NON (Fig. 8(d)), the
405 SDP-caused MLD increase is about ~3.4m. The order of magnitude of MLD at this stage
406 roughly coincides with that on 8 August, but MLD is generally deeper than that on 8
407 August, proving a hysteretic response between SDP and typhoon action.

408 At this stage, the circulation structure significantly differs from that at the
409 pre-typhoon stage on 7 August. As shown in Fig. 12(e), the main direction of currents on
410 10 August is eastward, flowing from the Liaodong Bay and the Bohai Bay to the Laizhou
411 Bay and the Bohai Strait, with relatively small speed in the Bohai Strait and the
412 Liaodong Bay. SDP mainly decreases the surface current speed in the northern Laizhou
413 Bay and the southern Bohai Strait (Fig. 12(g)), with the change ranging from 0.04 to
414 0.08m/s, demonstrating that the effect of Stokes drift is still persisting even after typhoon
415 left the study area. The difference rate (Fig. 12(h)) is generally reduced because of the
416 weakened winds, indicating that the impact of the Stokes drift on surface current is
417 largely related to wind speed. As the varying of wind, current is changed from the
418 surface deep down, forming a temporary current stratification (Fig. 9(g)). SDP promotes
419 the integral change in all depths, which makes the vertical distribution of currents more
420 uniformly (Fig. 9(h)), therefore weakens the stratification of flows.

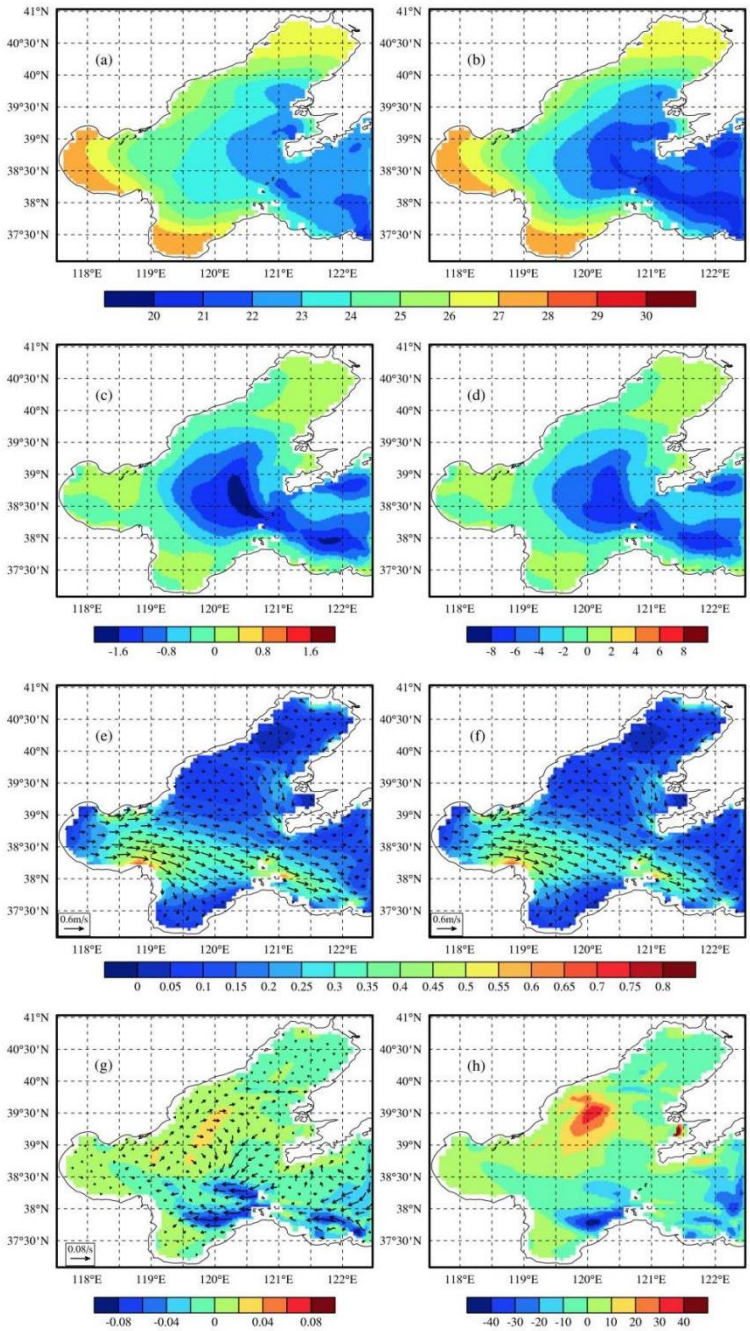

421

422 **Figure 12**. Horizontal distribution of (**a**) SST from WAVE-NON, (**b**) SST from
423 WAVE-ALL, (**c**) SST difference between WAVE-NON and WAVE-ALL, (**d**) SST
424 difference in percentage (%) between WAVE-NON and WAVE-ALL, (**e**) current from
425 WAVE-NON, (**f**) current from WAVE-ALL, (**g**) current difference between
426 WAVE-NON and WAVE-ALL, (**h**) current difference in percentage (%) between
427 WAVE-NON and WAVE-ALL at 0000UTC on 10 August 2005.

5 Conclusions

It is emphasized that the specific role of SDP in turbulent mixing and dynamics in BS under typhoon condition is rarely known, given that no study was focused on this issue as the infrequently visit of tropical storms to the region. Here we using an one-way coupled POMgcs-SWAN modeling system to investigate the influences of Stokes drift on mixing and dynamics for the first time in BS under typhoon condition. Case study of supertyphoon Matsa (2005) is comprehensively performed and presented.

At the pre-typhoon stage, the impacts of SDP on SST, MLD and current are relatively slight and the structures of temperature and current are generally similar to the normal weather situation that was discussed in our previous study (Cao & Deng, 2019). As Masta acting on the study area at the during-typhoon stage, the turbulent mixing is greatly improved by about 1 order of magnitude, demonstrating that high wind speed enables a large amount of TKE injection down to the deep. The difference between K_M and K_{MS} exceeds $0.008 m^2/s$, about 7 times that at the pre-typhoon stage, proving that the Stokes drift plays a significant role on turbulent mixing under typhoon condition. As a result, SSTs and current speed are greatly reduced, whereas MLD is increased. However, the vertical temperature structure is not substantially changed, and the TKE transmitted from the atmosphere to the ocean is mainly confined to the surface layer. The flows are vertically stratified, and noticeable speed difference exists between surface and deep layers. One day after the acting of strong typhoon winds, the Stokes drift brings deeper cold water up to the surface, leading to stronger surface cooling and weakened temperature stratification. The temperature differences caused by Stokes drift in the Central Area and the Bohai Strait are notable, with the maxima of more than 2°C (>10%), because the relatively large water depth in this region facilitates the pulling of deeper cold water to the surface by SDP effects. Numerical results show that in high wind speed situation, the Stokes drift-induced SST decrease can be altered by $\sim O(1)$. The vertical temperature structure is also changed greatly, accompanied by a generally increase in

455 MLD, except a rapid decrease near the center of the typhoon. The vertical distribution of
456 temperature tends to be more uniformly under the modulation of Stokes drift. Comparing
457 to the maximum current speed change of ~0.02m/s caused by Stokes drift under the
458 normal weather condition, the current speed is further reduced by over 0.2m/s at the
459 during-typhoon stage, which is about 10 times that of the normal weather case. The
460 maximum current change exceeds 100%, proving the notably influence of Stokes drift on
461 surface current during typhoon period. In addition, after adding SDP, current direction
462 change is generally opposite to the wind direction, suggesting that the Stokes drift
463 depresses the effect of high wind speed on currents by intensifying the vertical mixing.

464 At the after-typhoon stage, although strong wind is almost passed, the mixing is
465 still larger than that at pre-typhoon stage. The remained effect of SDP continuously
466 keeps the relatively low SST, and the alternations in SST magnitude and range are
467 similar to those at during-typhoon stage, indicating that SDP not only affects the SST at
468 synoptic time scale, but also impacts the total heat budget at longer time scales. The
469 Stokes drift-caused current speed change is decreased to 0.04~0.08m/s, and the
470 alternation in percentage is also generally reduced because of the weakened winds,
471 indicating that the impact of the Stokes drift on surface current is largely dependent on
472 wind speed. However, the change of current speed is still greater than that at the
473 pre-typhoon stage, and the change of current direction is opposite to the wind direction
474 as well. Besides, SDP continuously promotes the coordinated changes at all depths,
475 making the currents more uniformly in the vertical.

476 The combination impacts of SDP (CSF, LC, CLVF) on turbulent mixing as well
477 as ocean dynamics under typhoon conditions are comprehensively analyzed and
478 discussed. It's manifestly illustrated that SDP is of great significance to ocean dynamical
479 processes, in particular in typhoon weather. The impacts of these wave processes on
480 ocean dynamics are essential to improve ocean prediction and disaster forecasting. In the
481 actual ocean environment, the atmosphere, wave and circulation are always coupled, but

here we only have an one-way coupled model. In the future, the fully coupled atmosphere-circulation-wave model can be further developed to study the influences of SDP on ocean dynamics in BS under typhoon condition. In addition, SDP not only affects the physical processes, but also alters the distributions of organics and nutrients in the ocean. Therefore, the role of SDP in the ocean bio-ecological processes should be an interesting topic for further research.

Acknowledgments

This work was supported by: Foundation from Key Laboratory of Digital Ocean, Ministry of Natural Resources of China; Key Foundation from the Ministry of Education, China (Nos. 18JZD059); National Key Research and Development Program (2018YFC1407406); Foundation from Key Laboratory of Marine Environmental Information Technology, Ministry of Natural Resources of China; Foundation from Tianjin Municipal Transportation Commission (2020-14). All data generated or analysed during this study have been deposited in the Marine Data Archive database (https://mda.vliz.be/directlink.php?fid=VLIZ_00000960_5fd6dd2401ffc173595048). Requests for material should be made to the corresponding author.

Reference

Babanin, A. V., & Haus, B. K. (2009). On the Existence of Water Turbulence Induced by Nonbreaking Surface Waves. *Journal of Physical Oceanography*, 39(10), 2675–2679. https://doi.org/10.1175/2009JPO4202.1

Belcher, S. E., Grant, A. L. M., Hanley, K. E., Fox-Kemper, B., Van Roekel, L., Sullivan, P. P., et al. (2012). A global perspective on Langmuir turbulence in the ocean surface boundary layer: FRONTIER. *Geophysical Research Letters*, 39(18). https://doi.org/10.1029/2012GL052932

Blair, A., Ginis, I., Hara, T., & Ulhorn, E. (2017). Impact of Langmuir Turbulence on Upper Ocean Response to Hurricane Edouard: Model and Observations. *Journal of Geophysical Research: Oceans*, 122(12), 9712–9724. https://doi.org/10.1002/2017JC012956

Blumberg, A. F., & Mellor, G. L. (1987). A description of a three-dimensional coastal ocean circulation model. In N. S. Heaps (Ed.), *Coastal and Estuarine Sciences* (Vol. 4, pp. 1–16). Washington, D. C.: American Geophysical Union. https://doi.org/10.1029/CO004p0001

Carniel, S., Warner, J. C., Chiggiato, J., & Sclavo, M. (2009). Investigating the impact of surface wave breaking on modeling the trajectories of drifters in the northern Adriatic Sea during a wind-storm event. *Ocean Modelling*, 30(2–3), 225–239. https://doi.org/10.1016/j.ocemod.2009.07.001

Chu, P. C., & Cheng, K.-F. (2008). South China Sea wave characteristics during typhoon Muifa passage in winter 2004. *Journal of Oceanography*, 64(1), 1–21. https://doi.org/10.1007/s10872-008-0001-9

Craik, A. D. D., & Leibovich, S. (1976). A rational model for Langmuir circulations. *Journal of Fluid Mechanics*, 73(3), 401–426. https://doi.org/10.1017/S0022112076001420

D'Asaro, E. A., Thomson, J., Shcherbina, A. Y., Harcourt, R. R., Cronin, M. F., Hemer, M. A., & Fox-Kemper, B. (2014). Quantifying upper ocean turbulence driven by surface waves: QUANTIFYING SURFACE WAVE TURBULENCE. *Geophysical Research Letters*, 41(1), 102–107. https://doi.org/10.1002/2013GL058193

Deng, Z., Xie, L., Han, G., Zhang, X., & Wu, K. (2012). The effect of Coriolis-Stokes forcing on upper ocean circulation in a two-way coupled wave-current model. *Chinese Journal of Oceanology and Limnology*, 30(2), 321–335. https://doi.org/10.1007/s00343-012-1069-z

Dietrich, J. C., Zijlema, M., Westerink, J. J., Holthuijsen, L. H., Dawson, C., Luettich, R. A., et al. (2011). Modeling hurricane waves and storm surge using integrally-coupled,

scalable computations. *Coastal Engineering*, 58(1), 45–65. https://doi.org/10.1016/j.coastaleng.2010.08.001

Ezer, T., & Mellor, G. L. (2004). A generalized coordinate ocean model and a comparison of the bottom boundary layer dynamics in terrain-following and in z-level grids. *Ocean Modelling*, 6(3–4), 379–403. https://doi.org/10.1016/S1463-5003(03)00026-X

Fan, Y., Jarosz, E., Yu, Z., Rogers, W. E., Jensen, T. G., & Liang, J.-H. (2018). Langmuir turbulence in horizontal salinity gradient. *Ocean Modelling*, 129, 93–103. https://doi.org/10.1016/j.ocemod.2018.07.010

Gargett, A. E., & Wells, J. R. (2007). Langmuir turbulence in shallow water. Part 1. Observations. *Journal of Fluid Mechanics*, 576, 27–61. https://doi.org/10.1017/S0022112006004575

Garratt, J. (1977). Review of Drag Coefficients Over Oceans and Continents. *Monthly Weather Review*, 105, 915–929. https://doi.org/10.1175/1520-0493(1977)105<0915:RODCOO>2.0.CO;2

Grant, A., & Belcher, S. E. (2009). Characteristics of Langmuir Turbulence in the Ocean Mixed Layer. J. Phys. *Oceanogr.*, 39. https://doi.org/10.1175/2009JPO4119.1

Harcourt, R. (2015). An Improved Second-Moment Closure Model of Langmuir Turbulence. *Journal of Physical Oceanography*, 45, 84–103. https://doi.org/10.1175/JPO-D-14-0046.1

Harcourt, R., & D'Asaro, E. (2008). Large Eddy Simulation of Langmuir Turbulence in Pure Wind Seas. *Journal of Physical Oceanography*, 38. https://doi.org/10.1175/2007JPO3842.1

Harcourt, R. R. (2013). A Second-Moment Closure Model of Langmuir Turbulence. *Journal of Physical Oceanography*, 43(4), 673–697. https://doi.org/10.1175/JPO-D-12-0105.1

Hasselmann, K. (1970). Wave ‐ driven inertial oscillations. *Geophysical Fluid Dynamics*, 1(3–4), 463–502. https://doi.org/10.1080/03091927009365783

Holthuijsen, L., Powell, M., & Pietrzak, J. (2012). Wind and waves in extreme hurricanes. J Geophys Res 117:C09003. *Journal of Geophysical Research (Oceans)*, 117, 9003. https://doi.org/10.1029/2012JC007983

Hsu, J.-Y., Lien, R.-C., D'Asaro, E. A., & Sanford, T. B. (2017). Estimates of Surface Wind Stress and Drag Coefficients in Typhoon Megi. *Journal of Physical Oceanography*, 47(3), 545–565. https://doi.org/10.1175/JPO-D-16-0069.1

Huang, N. E. (1979). On surface drift currents in the ocean. *Journal of Fluid Mechanics*, 91(01), 191. https://doi.org/10.1017/S0022112079000112

Jones, B., de Ronde, C. E. J., & Renaut, R. W. (2008). Mineralized microbes from Giggenbach submarine volcano: SILICIFIED MICROBES. *Journal of Geophysical Research: Solid Earth*, 113(B8). https://doi.org/10.1029/2007JB005482

Kantha, L. H., & Anne Clayson, C. (2004). On the effect of surface gravity waves on mixing in the oceanic mixed layer. *Ocean Modelling*, 6(2), 101–124. https://doi.org/10.1016/S1463-5003(02)00062-8

Kukulka, T., Plueddemann, A. J., Trowbridge, J. H., & Sullivan, P. P. (2009). Significance of Langmuir circulation in upper ocean mixing: Comparison of observations and simulations. *Geophysical Research Letters*, 36(10), L10603. https://doi.org/10.1029/2009GL037620

Kukulka, T., Plueddemann, A. J., Trowbridge, J. H., & Sullivan, P. P. (2011). The influence of crosswind tidal currents on Langmuir circulation in a shallow ocean. *Journal of Geophysical Research*, 116(C8), C08005. https://doi.org/10.1029/2011JC006971

Kukulka, T., Plueddemann, A. J., & Sullivan, P. P. (2012). Nonlocal transport due to Langmuir circulation in a coastal ocean: LANGMUIR CIRCULATIONS IN A COASTAL OCEAN. *Journal of Geophysical Research: Oceans*, 117(C12), n/a-n/a. https://doi.org/10.1029/2012JC008340

Lane, E. M., Restrepo, J. M., & McWilliams, J. C. (2007). Wave–Current Interaction: A Comparison of Radiation-Stress and Vortex-Force Representations. *Journal of Physical Oceanography*, 37(5), 1122–1141. https://doi.org/10.1175/JPO3043.1

Langmuir, I. (1938). SURFACE MOTION OF WATER INDUCED BY WIND. *Science (New York, N.Y.)*, 87(2250), 119–123. https://doi.org/10.1126/science.87.2250.119

Large, W. G., McWilliams, J. C., & Doney, S. C. (1994). Oceanic vertical mixing: A review and a model with a nonlocal boundary layer parameterization. *Reviews of Geophysics*, 32(4), 363. https://doi.org/10.1029/94RG01872

Li, M., & Garrett, C. (1997). Mixed Layer Deepening Due to Langmuir Circulation. *Journal of Physical Oceanography - J PHYS OCEANOGR*, 27, 121–132.https://doi.org/10.1175/1520-0485(1997)027<0121:MLDDTL>2.0.CO;2

Li, Q., Webb, A., Fox-Kemper, B., Craig, A., Danabasoglu, G., Large, W. G., & Vertenstein, M. (2016). Langmuir mixing effects on global climate: WAVEWATCH III in CESM. *Ocean Modelling*, 103, 145–160. https://doi.org/10.1016/j.ocemod.2015.07.020

Li, S., Li, M., Gerbi, G. P., & Song, J.-B. (2013). Roles of breaking waves and Langmuir circulation in the surface boundary layer of a coastal ocean: BREAKING WAVES AND LANGMUIR CIRCULATION. *Journal of Geophysical Research: Oceans*, 118(10), 5173–5187. https://doi.org/10.1002/jgrc.20387

Li, Y., Peng, S., Wang, J., & Yan, J. (2014). Impacts of nonbreaking wave-stirring-induced mixing on the upper ocean thermal structure and typhoon intensity in the South China Sea. *Journal of Geophysical Research: Oceans*, 119(8), 5052–5070. https://doi.org/10.1002/2014JC009956

Longuet-Higgins, M. S., & Stewart, R. W. (1962). Radiation stress and mass transport in gravity waves, with application to 'surf beats.' *Journal of Fluid Mechanics*, 13(4), 481–504. https://doi.org/10.1017/S0022112062000877

Longuet-Higgins, M. S., & Stewart, R. w. (1964). Radiation stresses in water waves; a physical discussion, with applications. *Deep Sea Research and Oceanographic Abstracts*, 11(4), 529–562. https://doi.org/10.1016/0011-7471(64)90001-4

Mao, M., & Xia, M. (2016). Dynamics of wave–current–surge interactions in Lake Michigan: A model comparison. *Ocean Modelling*, 110. https://doi.org/10.1016/j.ocemod.2016.12.007

Mao, M., & Xia, M. (2018). Wave–current dynamics and interactions near the two inlets of a shallow lagoon–inlet–coastal ocean system under hurricane conditions. *Ocean Modelling*, 129, 124–144. https://doi.org/10.1016/j.ocemod.2018.08.002

McWILLIAMS, J. C., Sullivan, P. P., & Moeng, C.-H. (1997). Langmuir turbulence in the ocean. *Journal of Fluid Mechanics*, 334, 1–30. https://doi.org/10.1017/S0022112096004375

McWilliams, J. C., Huckle, E., Liang, J.-H., & Sullivan, P. P. (2012). The Wavy Ekman Layer: Langmuir Circulations, Breaking Waves, and Reynolds Stress. *Journal of Physical Oceanography*, 42(11), 1793–1816. https://doi.org/10.1175/JPO-D-12-07.1

McWilliams, J. C., Huckle, E., Liang, J., & Sullivan, P. P. (2014). Langmuir Turbulence in Swell. *Journal of Physical Oceanography*, 44(3), 870–890. https://doi.org/10.1175/JPO-D-13-0122.1

McWilliams, James, & Sullivan, P. (2000). Vertical Mixing by Langmuir Circulations. *Spill Science & Technology Bulletin*, 6, 225–237. https://doi.org/10.1016/S1353-2561(01)00041-X

McWilliams, JC, & Restrepo, J. (1999). The Wave-Driven Ocean Circulation. *Journal of Physical Oceanography*, 29, 2523–2540. https://doi.org/10.1175/1520-0485(1999)029<2523:TWDOC>2.0.CO;2

Mellor, G. (2005a). Some Consequences of the Three-Dimensional Current and Surface Wave Equations. *Journal of Physical Oceanography*, 35(11), 2291–2298. https://doi.org/10.1175/JPO2794.1

Mellor, G. (2005b). The Three-Dimensional Current and Surface Wave Equations. *J. Phys. Oceanogr.*, 33. https://doi.org/10.1175/JPO2794.1

651 Mellor, G. (2013). Waves, circulation and vertical dependence. *Ocean Dynamics*, 63(4),
652 447–457. https://doi.org/10.1007/s10236-013-0601-9

653 Mellor, G., & Yamada, T. (1982). Development of a Turbulent Closure Model for
654 Geophysical Fluid Problems. *Rev. Geophys. Space Phys.*, 20, 851–875. https://doi.org/10.
655 1029/RG020i004p00851

656 Noh, Y., Min, H. S., & Raasch, S. (2004). Large Eddy Simulation of the Ocean Mixed
657 Layer: The Effects of Wave Breaking and Langmuir Circulation. *Journal of Physical*
658 *Oceanography - J PHYS OCEANOGR*, 34. https://doi.org/10.1175/1520-0485(2004)
659 034<0720:LESOTO>2.0.CO;2

660 Noh, Y., Goh, G., & Raasch, S. (2011). Influence of Langmuir Circulation on the
661 Deepening of the Wind-Mixed Layer. *Journal of Physical Oceanography - J PHYS*
662 *OCEANOGR*, 41, 472–484. https://doi.org/10.1175/2010JPO4494.1

663 Noh, Y., Ok, H., Lee, E., Toyoda, T., & Hirose, N. (2016). Parameterization of
664 Langmuir Circulation in the Ocean Mixed Layer Model Using LES and Its Application
665 to the OGCM. *Journal of Physical Oceanography*, 46(1), 57–78. https://doi.org/10.
666 1175/JPO-D-14-0137.1

667 Pearson, B. C., Grant, A. L. M., Polton, J. A., & Belcher, S. E. (2015). Langmuir
668 Turbulence and Surface Heating in the Ocean Surface Boundary Layer. *Journal of*
669 *Physical Oceanography*, 45(12), 2897–2911. https://doi.org/10.1175/JPO-D-15-0018.1

670 Polton, J. A., & Belcher, S. E. (2007). Langmuir turbulence and deeply penetrating jets
671 in an unstratified mixed layer. *Journal of Geophysical Research*, 112(C9), C09020.
672 https://doi.org/10.1029/2007JC004205

673 Polton, J. A., Lewis, D. M., & Belcher, S. E. (2005). The Role of Wave-Induced
674 Coriolis–Stokes Forcing on the Wind-Driven Mixed Layer. *Journal of Physical*
675 *Oceanography*, 35(4), 444–457. https://doi.org/10.1175/JPO2701.1

676 Powell, M. D., Vickery, P. J., & Reinhold, T. A. (2003). Reduced drag coefficient for
677 high wind speeds in tropical cyclones. *Nature*, 422(6929), 279–283. https://doi.org/10.
678 1038/nature01481

679 Rabe, T. J., Kukulka, T., Ginis, I., Hara, T., Reichl, B. G., D'Asaro, E. A., et al. (2015).
680 Langmuir Turbulence under Hurricane Gustav (2008). *Journal of Physical*
681 *Oceanography*, 45(3), 657–677. https://doi.org/10.1175/JPO-D-14-0030.1

682 Reichl, B. G., Ginis, I., Hara, T., Thomas, B., Kukulka, T., & Wang, D. (2016). Impact
683 of Sea-State-Dependent Langmuir Turbulence on the Ocean Response to a Tropical
684 Cyclone. *Monthly Weather Review*, 144(12), 4569–4590. https://doi.org/10.1175/
685 MWR-D-16-0074.1

Reichl, B. G., Wang, D., Hara, T., Ginis, I., & Kukulka, T. (2016). Langmuir Turbulence Parameterization in Tropical Cyclone Conditions. *Journal of Physical Oceanography*, 46(3), 863–886. https://doi.org/10.1175/JPO-D-15-0106.1

Skyllingstad, E. D., & Denbo, D. W. (1995). An ocean large-eddy simulation of Langmuir circulations and convection in the surface mixed layer. *Journal of Geophysical Research*, 100(C5), 8501. https://doi.org/10.1029/94JC03202

Sullivan, P. P., McWILLIAMS, J. C., & Melville, W. K. (2007). Surface gravity wave effects in the oceanic boundary layer: large-eddy simulation with vortex force and stochastic breakers. *Journal of Fluid Mechanics*, 593, 405–452. https://doi.org/10.1017/S002211200700897X

Sullivan, P. P., Romero, L., McWilliams, J. C., & Melville, W. K. (2012). Transient Evolution of Langmuir Turbulence in Ocean Boundary Layers Driven by Hurricane Winds and Waves. *Journal of Physical Oceanography*, 42(11), 1959–1980. https://doi.org/10.1175/JPO-D-12-025.1

Sun, F. (2004). Wave-induced stress and estimation of its driven effect on currents. *Science in China Series D*, 47(12), 1147. https://doi.org/10.1360/02yd0292

Thorpe, S. A. (1984). The effect of Langmuir circulation on the distribution of submerged bubbles caused by breaking wind waves. *Journal of Fluid Mechanics*, 142, 151–170. https://doi.org/10.1017/S0022112084001038

Van Roekel, L. P., Fox-Kemper, B., Sullivan, P. P., Hamlington, P. E., & Haney, S. R. (2012). The form and orientation of Langmuir cells for misaligned winds and waves: LANGMUIR UNDER MISALIGNED WIND AND WAVES. *Journal of Geophysical Research: Oceans*, 117(C5), n/a-n/a. https://doi.org/10.1029/2011JC007516

Wang, D., Kukulka, T., Reichl, B. G., Hara, T., Ginis, I., & Sullivan, P. P. (2018). Interaction of Langmuir Turbulence and Inertial Currents in the Ocean Surface Boundary Layer under Tropical Cyclones. *Journal of Physical Oceanography*, 48(9), 1921–1940. https://doi.org/10.1175/JPO-D-17-0258.1

Wang, Z., Wu, K., Dong, S., Deng, Z., & Zhang, X. (2015). Effect of wave-induced Stokes drift on the dynamics of ocean mixed layer. *Chinese Journal of Oceanology and Limnology*, 33(1), 233–242. https://doi.org/10.1007/s00343-015-4036-7

Webb, A., & Fox-Kemper, B. (2011). Wave spectral moments and Stokes drift estimation. *Ocean Modelling*, 40(3–4), 273–288. https://doi.org/10.1016/j.ocemod.2011.08.007

Wu, J. (1982). Wind-stress coefficients over sea surface from breeze to hurricane. *Journal of Geophysical Research*, 87(C12), 9704. https://doi.org/10.1029/JC087iC12p09704

722 Wu, L., Rutgersson, A., & Sahlée, E. (2015). Upper - ocean mixing due to surface
723 gravity waves. *Journal of Geophysical Research: Oceans*, 120(12), 8210–8228. https://
724 doi.org/10.1002/2015JC011329

725 Zhang, L., Zhang, X., Chu, P. C., Guan, C., Fu, H., Chao, G., et al. (2017). Impact of sea
726 spray on the Yellow and East China Seas thermal structure during the passage of
727 Typhoon Rammasun (2002): IMPACT OF SEA SPRAY ON UPPER OCEAN. *Journal*
728 *of Geophysical Research: Oceans*, 122(10), 7783–7802. https://doi.org/10.1002/
729 2016JC012592

730 Zhang, X., Han, G., Wang, D., Deng, Z., & Li, W. (2012). Summer surface layer thermal
731 response to surface gravity waves in the Yellow Sea. *Ocean Dynamics*, 62(7), 983–1000.
732 https://doi.org/10.1007/s10236-012-0547-3

733 Zhang, X., Chu, P. C., Li, W., Liu, C., Zhang, L., Shao, C., et al. (2018). Impact of
734 Langmuir Turbulence on the Thermal Response of the Ocean Surface Mixed Layer to
735 Supertyphoon Haitang (2005). *Journal of Physical Oceanography*, 48(8), 1651–1674.
736 https://doi.org/10.1175/JPO-D-17-0132.1

737 Zhao, Y., Deng, Z., Yu, T., & Wang, H. (2019). Numerical Study on Tidal Mixing in the
738 Bohai Sea. *Marine Geodesy*, 42(1), 46–63. https://doi.org/10.1080/
739 01490419.2018.1539055

740 Zijlema, M., van Vledder, G. Ph., & Holthuijsen, L. H. (2012). Bottom friction and wind
741 drag for wave models. *Coastal Engineering*, 65, 19–26. https://doi.org/10.1016/j.
742 coastaleng.2012.03.002

743